Radiology Case Reports 19 (2024) 4963–4969

Available online at www.sciencedirect.com

ScienceDirect

journal homepage: www.elsevier.com/locate/radcr

Case Report

Pulmonary metastases of a renal angiomyolipoma: A case report, with whole-exome sequencing analysis ☆

Yuki Sonoda[a,*], *Masataka Hirasaki*[b], *Yoko Usami*[a], *Tomoaki Torigoe*[c], *Tomonori Kawasaki*[d], *Nobuyuki Suzuki*[d], *Yukihiro Shiraki*[e], *Atsushi Enomoto*[e], *Hiroki Imada*[f], *Yasutaka Baba*[a]

[a] *Department of Diagnostic Radiology, Saitama Medical University International Medical Centre, 1397-1, Yamane, Hidaka, Saitama 350-1298 Japan*
[b] *Department of Clinical Cancer Genomics, Saitama Medical University International Medical Centre, 1397-1, Yamane, Hidaka, Saitama 350-1298 Japan*
[c] *Department of Orthopaedic Oncology, Saitama Medical University International Medical Centre, 1397-1, Yamane, Hidaka, Saitama 350-1298 Japan*
[d] *Department of Pathology, Saitama Medical University International Medical Centre, 1397-1, Yamane, Hidaka, Saitama 350-0495 Japan*
[e] *Department of Pathology, Nagoya University Graduate School of Medicine, 65 Tsurumai-cho, Showa-ku, Nagoya 466-8550 Japan*
[f] *Department of Pathology, Saitama Medical University, Saitama Medical Centre, 1981, Kamoda, Kawagoe, Saitama 350-8550 Japan*

ARTICLE INFO

Article history:
Received 24 June 2024
Accepted 19 July 2024

Keywords:
Angiomyolipoma
Lung
Multicentric
Metastatic
Mosaicism
Whole-exome sequencing

ABSTRACT

We present a case of pulmonary metastasis originating from renal angiomyolipoma (AML), as evidenced by whole-exome sequencing (WES) analysis. Although AML predominantly arises in the kidneys, it can emerge in various body parts, making it important to distinguish between multicentric development and metastasis. However, previous studies have not distinguished between these conditions. Our case features an 82-year-old woman with a history of renal AML who presented with multiple, randomly distributed, bilateral pulmonary nodules of varying size and pure fat densities. The patient's condition followed a benign course over 10 years. Through WES, we discovered shared mutations in pulmonary lesions that were absent in the patient's blood, including a pathological mutation in TSC2, suggesting a metastatic origin from renal AML. Knowledge of the pulmonary manifestations of AML and their distinctive imaging findings can help radiologists and clinicians diagnose and manage patients with similar presentations.

☆ Competing Interests: We declare that we have no conflict of interest.

* Corresponding author.
E-mail address: ysonoda.diagrad@gmail.com (Y. Sonoda).

https://doi.org/10.1016/j.radcr.2024.07.113

Introduction

Angiomyolipoma (AML) is a benign tumor thought to originate from the perivascular epithelial cells that surround the blood vessels. Although the kidneys are the most frequent site for AML occurrence, lesions have been identified in various other locations, including the mediastinum, uterus, vagina, fallopian tube, spermatic cord, penis, hard palate, abdominal wall, retroperitoneum, and lymph nodes [1,2].

Pulmonary manifestations of AML are extremely rare, with only 11 reported cases [3–13]. Eight of these cases reported the coexistence of AML with lesions in other organs [4,6–9,11–13]. Tumor lesions in a particular organ with lesions of similar tissue type in the lungs, typically raise the presumption of metastases. However, given that perivascular epithelial cells are ubiquitous, and that AML can theoretically arise anywhere, the presence of AMLs in multiple organs raises the possibility of multicentric occurrence or metastasis. Previous case reports have not successfully differentiated between multicentric occurrence and metastasis.

This case report presents the pathological findings and whole-exome sequencing (WES) analysis of AMLs in the patient's lungs and kidneys. We discuss how these findings suggest that lung AMLs are likely to be metastatic tumors in this case.

Case report

An 82-year-old woman was referred for evaluation of multiple lung nodules discovered during a routine health checkup. Her medical history included a right mastectomy for breast cancer at the age of 60 years, and hypothyroidism managed with levothyroxine. Physical examination revealed a surgical scar on the right side of the chest. No other skin lesions were observed. The neurological findings were normal. The patient had no relevant family history.

Contrast-enhanced chest computed tomography (CT) revealed multiple well-defined bilateral lung nodules with a lipid density measuring up to 15 mm, without calcification or enhancement. The nodules exhibited a random distribution pattern (Fig. 1). A contrast-enhanced abdominal CT revealed a large fat-containing mass located in the retroperitoneum adjacent to the inferior pole of the right kidney (Fig. 2). The mass appeared to be well-defined and heterogeneous, exhibiting both lipid and soft tissue densities. A vascular-like structure extending towards the right kidney was observed during the early phase of the dynamic study. Additionally, the right inferior contour of the right kidney adjacent to the tumor displayed a wedged shape. Fluorine-18-fluorodeoxyglucose (FDG) positron emission tomography revealed minimal FDG uptake in the retroperitoneal and pulmonary lesions, with no abnormal FDG accumulation detected elsewhere in the body.

An open biopsy of the lung lesions with a wedge resection of the left upper lobe of the lung was performed. Histological analysis of the lung lesions revealed the presence of 9 AML lesions, measuring up to 12 mm in the sample (Fig. 3). Core-needle biopsy of the retroperitoneal mass confirmed the histological diagnosis of AML. Based on the localized presentation, the AML was considered to be of renal origin. The lesion did not exhibit cellular atypia or features of epithelioid AML.

Following the surgery, it was discovered that the patient had been undergoing radiological monitoring of the pulmonary and retroperitoneal lesions at another hospital for a period spanning from 11 to 7 years before the operation. However, clinical information from that period was unavailable, and the patient failed to recall any details. Nevertheless, a review of these previous CT scans revealed a progressive increase in the size of the pulmonary nodules. The largest pulmonary nodule grew from 6 mm to 15 mm over 11 years.

Genetic testing for TSC1 and TSC2 mutations in the patient's whole blood was negative, and apart from multiple AMLs, there were no physical findings consistent with tuberous sclerosis. Three years after the lesions were discovered, the patient remained asymptomatic, and the sizes of both the renal and pulmonary AML lesions remained unchanged.

WES was conducted to identify somatic variants present in the lung lesions and absent in the patient's blood sample, thereby confirming whether the lung lesions were multicentric or metastatic in origin. Genomic DNA was extracted from 2 microdissected lung lesions, which were preserved in formalin-fixed paraffin-embedded (FFPE) tissue, and from a blood sample using Maxwell® Rapid Sample Concentrator DNA FFPE Kit (Promega, Madison, WI, USA) for pulmonary lesions, and the Maxwell® Rapid Sample Concentrator Blood DNA Kit (Promega, Madison, WI, USA) for blood samples.

Fig. 1 – Chest contrast-enhanced CT shows multiple pulmonary nodules up to 15 mm in size with clear margins and homogeneous internal characteristics, distributed bilaterally in a random pattern in the lungs. In the mediastinal window, the internal density of the nodule (arrow) is -110 Hounsfield units, indicative of significant fat content, with no evident contrast enhancement in the nodules.

Table 1 – Shared gene mutations were identified in 2 pulmonary AML lesions by whole-exome sequencing.

Gene symbol	ExonicFunc.refGene	Nucleotide change	Aa change	EX_M087_001			EX_M087_002		
				RefSeq count	AltSeq count	VAF	RefSeq count	AltSeq count	VAF
BTBD3	nonsynonymous SNV	NM_014962:c.205C>A	p.R69S	69	2	0.029	52	2	0.0385
CHCHD6	nonsynonymous SNV	NM_001320610:c.599G>A	p.G200E	297	15	0.0505	266	12	0.0451
CHST4	synonymous SNV	NM_001166395:c.984T>A	p.L328L	156	6	0.0385	148	8	0.0541
COMMD7	nonsynonymous SNV	NM_001099339:c.434G>A	p.G145E	293	6	0.0205	256	2	0.0078
DST	nonsynonymous SNV	NM_001723:c.450A>T	p.L150F	59	2	0.0339	62	1	0.0161
DYNC2H1	synonymous SNV	NM_001080463:c.3072T>C	p.S1024S	73	2	0.0274	40	4	0.1
FN1	nonsynonymous SNV	NM_001306129:c.76G>T	p.A26S	464	2	0.0043	412	2	0.0049
GCSH	synonymous SNV	NM_004483:c.33C>T	p.A11A	27	6	0.2222	34	1	0.0294
GFM2	nonsynonymous SNV	NM_001281302:c.41C>T	p.T14M	229	1	0.0044	207	3	0.0145
GLIS3	synonymous SNV	NM_152629:c.516G>A	p.L172L	428	16	0.0374	386	9	0.0233
GPR68	synonymous SNV	NM_001177676:c.166C>T	p.L56L	221	9	0.0407	249	15	0.0602
HINFP	frameshift deletion	NM_001351963:c.171_183del	p.C58Pfs*132	314	23	0.0732	331	5	0.0151
KMT2D	synonymous SNV	NM_003482:c.1938C>A	p.P646P	200	2	0.01	197	2	0.0102
LNP1	nonsynonymous SNV	NM_001085451:c.230G>A	p.R77Q	46	2	0.0435	48	2	0.0417
MXRA7	synonymous SNV	NM_001008528:c.21A>C	p.L7L	52	32	0.6154	67	20	0.2985
PDSS1	nonsynonymous SNV	NM_001321979:c.364G>A	p.A122T	33	2	0.0606	31	2	0.0645
PLSCR2	nonsynonymous SNV	NM_001199979:c.52C>T	p.P18S	150	3	0.02	142	4	0.0282
PLXNA2	nonsynonymous SNV	NM_025179:c.2292C>A	p.N764K	160	12	0.075	143	1	0.007
PLXNA3	synonymous SNV	NM_017514:c.3279G>A	p.A1093A	480	27	0.0563	461	14	0.0304
RGL1	nonsynonymous SNV	NM_001297670:c.568C>T	p.L190F	70	3	0.0429	76	3	0.0395
SLC35F3	nonsynonymous SNV	NM_001300845:c.875A>G	p.E292G	55	5	0.0909	59	1	0.0169
SPAG17	nonsynonymous SNV	NM_206996:c.613G>A	p.D205N	108	2	0.0185	74	1	0.0135
TMEM151B	synonymous SNV	NM_001137560:c.96G>A	p.A32A	46	2	0.0435	53	2	0.0377
TSC2	frameshift deletion	NM_001318831:c.1569_1573del	p.T525Pfs*35	299	8	0.0268	246	1	0.0041
ZNF208	nonsynonymous SNV	NM_007153:c.3247G>A	p.E1083K	134	6	0.0448	97	4	0.0412
ZRANB3	stopgain	NM_001286568:c.1288C>T	p.R430X	18	3	0.1667	20	1	0.05

ExonicFunc.refGene: Effect of mutation on coding region. Nucleotide change: Mutation at nucleotide level. Aa change: Mutation at amino acid level. RefSeq count: Number of reads supporting reference allele. AltSeq count: Number of reads supporting mutant allele. VAF (Variant Allele Frequency): Frequency of mutant allele.

and the DNA was subsequently purified using The Maxwell® Rapid Sample Concentrator Instrument (Promega, Madison, WI, USA).

Exome enrichment was performed using the SureSelect Human All Exon V8 kit (Agilent Technologies, Santa Clara, CA, USA), followed by sequencing using the NovaSeq 6000 system (Illumina, San Diego, CA, USA) by Riken Genesis (Tokyo, Japan). GATK Mutect2 was used to detect somatic SNVs and INDELs, using the blood sample as a reference. Variants were filtered using GATK FilterMutectCalls and annotated with ANNOVAR [14]. We identified 35 and 36 genetic alterations in the 2 lung samples EX_M087_001 and EX_M087_002, respectively (Table 1). Of these alterations, 26 were shared between both samples, including 2 frameshift deletions, 14 nonsynonymous SNVs, 1 stopgain, and 9 synonymous SNVs (Table 2). Notably, both samples harbored a common frameshift deletion in the TSC2 gene.

Discussion

In this study, we present the case of an 82-year-old woman with multiple lung and renal AML. This case highlights

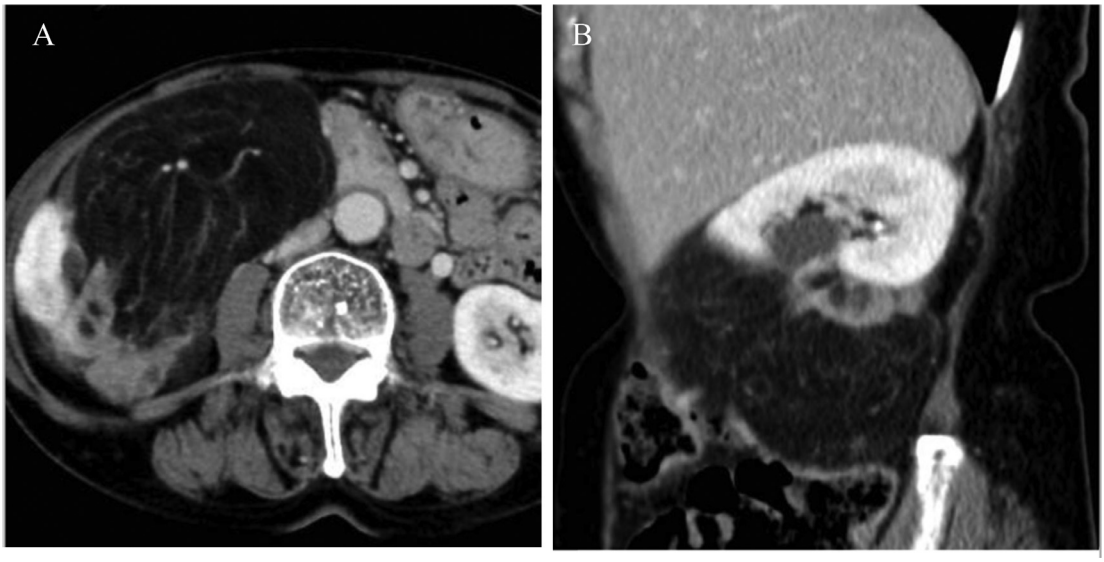

Fig. 2 – Contrast-enhanced CT reveals a soft tissue density lesion with coarse fat components at the right renal lower pole. Dilated vascular-like structures are apparent within the fat, and the right renal lower pole exhibits a wedge-shaped deformation, enlarging towards the renal hilum.

Table 2 – Mutations found exclusively in lung lesions, categorized by mutation type.

	Number of mutations shared between lung lesions	Total number of mutations
frameshift deletion	2	2
splicing	0	1
nonframeshift deletion	0	3
nonsynonymous SNV	14	22
stopgain	1	2
synonymous SNV	9	14

2 important findings: 1) WES analysis identified a shared frameshift deletion in the TSC2 gene in the 2 lung lesions, which was absent in the patient's blood sample, and 2) pulmonary AMLs followed a benign clinical course.

Previous studies have indicated that the biallelic loss of TSC1 or TSC2 is a key and sufficient trigger for the development of renal AML [15]. Mechanisms underlying allele loss include germline mutations, mosaicism, somatic mutations, and loss of heterozygosity. TSC1 and TSC2 genes encode proteins that serve as negative regulators of the mammalian target of the rapamycin (mTOR) pathway. Loss-of-function mutations in both alleles of one of these genes result in hyperactivation of the mTOR pathway, leading to uncontrolled cell proliferation.

Tuberous sclerosis complex is characterized by the formation of benign hamartomas across various organs, with most patients exhibiting germline mutations in pathogenic variants of TSC1/TSC2. However, approximately 10% of patients do not show pathogenic variants of TSC1/TSC2 in the blood through standard genetic testing, suggesting the presence of mosaic pathogenic variants in these genes [16].

In the present case, WES analysis identified a shared frameshift deletion in TSC2 across the 2 pulmonary nodules, which was absent in the blood sample. This finding suggests 2 possible scenarios: either the patient has mosaic TSC2 mutations, with pulmonary tumors harboring the same mutations, or the renal AML has metastasized to the lungs. The identification of 9 AML lesions in a partial resection of the right upper lobe, coupled with the expectation of additional lesions in both lungs, suggests that metastasis is a more likely scenario. This is further supported by the growth rate of these tumors and their emergence in old age. A mosaic scenario implies the independent and nearly simultaneous emergence of pathological mutations in the unaffected alleles of TSC2 across numerous lung lesions, presenting for the first time in an elderly individual. Consequently, the pulmonary AMLs in this case were suspected to be metastatic renal AML.

To conclusively differentiate between multicentric occurrence and metastasis, it is crucial to demonstrate that the genetic alterations affecting both TSC2 alleles, i.e. the first and second hits, are identical in the lung and kidney AMLs. However, the limited quantity of renal biopsy material prevented the application of WES to renal AML samples, representing one of the limitations of this study. Moreover, the lung specimens were preserved in FFPE format, restricting next-generation sequencing to detecting only short reads. This

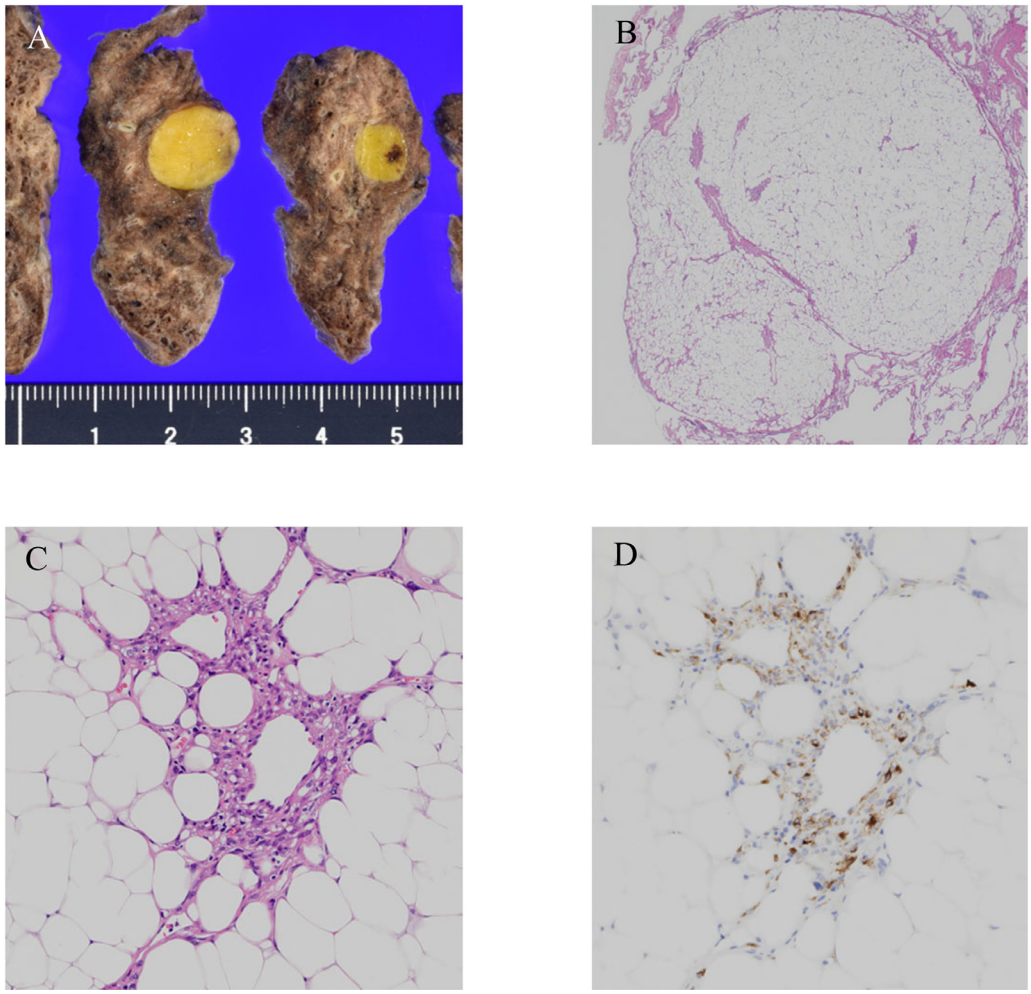

Fig. 3 – (A) Gross pathology of the lung nodules. (B) The partially resected lung specimen contains a "lipoma-like" lobulated mass, predominantly composed of adipose tissue (H&E, x 20). (C) On a high-power view, this tumour shows spindle cell proliferation surrounded by abundant, mature fat cells (x 200). (D) These spindle cells are inhomogeneously immunopositive for HMB45 (x 200).

poses another limitation to the study, as it hinders comprehensive analyses of large-scale genomic alterations, including copy number variations and structural variations, within the TSC2 region. Preserving surgical specimens as freshly frozen samples is considered advantageous to enable such in-depth analyses in the future.

To date, 11 cases of pulmonary AML have been documented in English literature (Table 3). These reports describe the characteristic imaging findings of pulmonary AML, including well-defined margins, homogeneous appearance, lack of enhancement, and pure fat density. Among these, 3 cases involved a single or 2 lung lesions without AMLs in other organs [3,5,10], suggesting that pulmonary AML can occur in isolation. One case described a patient with tuberous sclerosis who had 1 pulmonary AML, bilateral renal AMLs, and multiple hamartomatous lesions in various organs that were identified at autopsy [6]. The remaining 7 cases featured multiple pulmonary AML nodules, with concurrent liver lesions in 2 cases [7,9], a mediastinal lesion in 1 case [12], and renal lesions in 6 cases [4,8,11–13], all of which had a previous history of nephrectomy. Except for 1 postmortem case, all reported instances of pulmonary AML have shown favorable outcomes, consistent with the prognosis in the current case.

The differential diagnosis of a retroperitoneal tumor containing fat typically includes lipomas, liposarcomas, and AML. The identification of a vascular structure leading towards the kidney and a wedge-shaped contour defect in the kidney strongly suggest AML [17], as was demonstrated in the present case. The differential diagnoses of fat-containing pulmonary nodules are limited and include pulmonary hamartoma, lipoma, myelolipoma, metastatic liposarcoma, and metastatic renal cell carcinoma [18]. In the present case, the patient had no history or diagnostic findings suggestive of liposarcoma or renal cell carcinoma. Considering the strong concordance between the imaging findings in this case and the previously reported presentation of pulmonary AML, a precise diagnosis could have been made based on radiological evidence, eliminating the need for invasive procedures, such as biopsy or surgery.

Table 3 – Previously reported cases and the present case of pulmonary AML.

No.	Authours	Sex/Age	Number of pulmonary AMLs	AML involvement of other organs	TSC	Other notes
1	Guinee et al. [3]	F/68	1	-	-	-
2	Maffezzini et al. [4]	F/42	2	Kidney	+	Status post nephrectomy
3	Ito et al. [5]	M/67	1	-	-	-
4	Wu et al. [6]	F/36	Multiple	Kidney(s)	+	Autopsy case Hamartomatous tumors associated with TSC in multiple organs are noted
5	Garcia et al. [7]	F/50	Multiple	Liver	-	-
6	Kasuno et al. [8]	F/57	Multiple	Kidney, spleen	-	Status post nephrectomy
7	Saito et al. [9]	F/57	Multiple	Liver	-	Status post hepatectomy
8	Marcheix et al. [10]	F/63	1	-	-	-
9	Hino et al. [11]	F/52	Multiple	Kidney	-	Status post nephrectomy
10	Morita et al. [12]	F/56	Multiple	Kidney, mediastinum	+	Status post nephrectomy, concurrent lymphangioleiomatosis
11	Sun et al. [13]	F/38	Multiple	Kidney	+	Status post nephrectomy, concurrent lymphangioleiomatosis
12	Present case	F/82	Multiple	Kidney	-	-

TSC: tuberous sclerosis complex;
+ indicates the presence of TSC as explicitly stated in the original report, while—denotes either the absence of TSC or no mention of TSC in the report.

Conclusion

This report presents a case that strongly suggests pulmonary metastasis of AML, supported by WES findings demonstrating shared mutations in the lung lesions that were absent from the patient's blood sample. Despite the metastatic nature of the lesions, they exhibited pathological features consistent with benign behavior. Recognizing the pulmonary manifestations of AML and their distinctive imaging findings, including well-defined margins, homogeneous appearance, lack of enhancement, and pure fat density, in the presence of AML in another organ may allow for sparing invasive diagnostic procedures and enable appropriate management of future cases with similar presentations. This case highlights the importance of increased awareness of pulmonary AML among radiologists and clinicians and the need for further research to better understand the metastatic potential of AML and the utility of WES in guiding diagnosis.

IRB approval

The research protocol was reviewed and approved by the Institutional Review Board of Saitama Medical University International Medical Center.

Patient consent

Written informed consent was obtained from the study participant.

REFERENCES

[1] Castillenti TA, Bertin AP. Angiomyolipoma of the spermatic cord: case report and literature review. J Urol 1989;142:1308–9. doi:10.1016/s0022-5347(17)39068-7.
[2] Ansari SJ, Stephenson RA, Mackay B. Angiomyolipoma of the kidney with lymph node involvement. Ultrastruct Pathol 1991;15:531–8. doi:10.3109/01913129109016260.
[3] Guinee DG, Thornberry DS, Azumi N, Przygodzki RM, Koss MN, Travis WD. Unique pulmonary presentation of an angiomyolipoma: analysis of clinical, radiographic, and histopathologic features. Am J Surg Pathol 1995;19:476–80. doi:10.1097/00000478-199504000-00010.
[4] Maffezzini M, Vlassopoulos G, Simonato A, Bussani R, Silvestri F, Carmignani G. Renal angiomyolipoma with extrarenal involvement—in vascular, lymph-node and perirenal tissue: reports of four cases. Scand J Urol Nephrol 1995;29:327–9. doi:10.3109/00365599509180584.
[5] Ito M, Sugamura Y, Ikari H, Sekine I. Angiomyolipoma of the lung. Arch Pathol Lab Med 1998;122:1023–5.
[6] Wu K, Tazelaar HD. Pulmonary angiomyolipoma and multifocal micronodular pneumocyte hyperplasia associated with tuberous sclerosis. Hum Pathol 1999;30:1266–8. doi:10.1016/s0046-8177(99)90049-7.
[7] Rivera Garcia T, Mestre De Juan MJ. Angiomyolipoma of the liver and lung: a case explained by the presence of perivascular epithelioid cells. Pathology - Research and Practice 2002;198:363–7. doi:10.1078/0344-0338-00267.
[8] Kasuno K, Ueda S, Tanaka A, Tanaka-Kasuno Y, Kuwahara T. Pulmonary angiomyolipoma recurring 26 years after nephrectomy for angiomyolipoma: benign clinical course. CN 2004;62:469–72. doi:10.5414/CNP62469.
[9] Saito M, Tsukamoto T, Takahashi T, Sai K, Fujii H, Nagashima K. Multifocal angiomyolipoma affecting the liver and lung without tuberous sclerosis. J Clin Pathol 2004;57:221–4.

[10] Marcheix B, Brouchet L, Lamarche Y, Renaud C, Gomez-Brouchet A, Hollington L, et al. Pulmonary angiomyolipoma. Ann Thorac Surg 2006;82:1504–6.
[11] Hino H, Ikeda S, Kawano R, Sato F, Tagawa K, Hoshino T, et al. Angiomyolipoma in the lung detected 15 years after a nephrectomy for renal angiomyolipoma. Ann Thorac Surg 2010;89:298–300.
[12] Morita K, Shida Y, Shinozaki K, Uehara S, Seto T, Sugio K, et al. Angiomyolipomas of the mediastinum and the lung. J Thorac Imaging 2012;27:W21–3. doi:10.1097/RTI.0b013e31823150c7.
[13] Northrup H, Krueger DA, Northrup H, Krueger DA, Roberds S, Smith K, et al. Tuberous sclerosis complex diagnostic criteria update: Recommendations of the 2012 International Tuberous Sclerosis Complex Consensus Conference. Pediatr Neurol 2013;49:243–54. doi:10.1016/j.pediatrneurol.2013.08.001.
[14] Wang K, Li M, Hakonarson H. ANNOVAR: functional annotation of genetic variants from high-throughput sequencing data. Nucleic Acids Res 2010;38:e164.
[15] Giannikou K, Malinowska IA, Pugh TJ, Yan R, Tseng Y-Y, Oh C, et al. Whole exome sequencing identifies TSC1/TSC2 biallelic loss as the primary and sufficient driver event for renal angiomyolipoma development. PLoS Genet 2016;12:e1006242. doi:10.1371/journal.pgen.1006242.
[16] Ye Z, Lin S, Zhao X, Bennett MF, Brown NJ, Wallis M, et al. Mosaicism in tuberous sclerosis complex: lowering the threshold for clinical reporting. Hum Mutat 2022;43:1956–69. doi:10.1002/humu.24454.
[17] Israel GM, Bosniak MA, Slywotzky CM, Rosen RJ. CT differentiation of large exophytic renal angiomyolipomas and perirenal liposarcomas. AJR Am J Roentgenol 2002;179:769–73. doi:10.2214/ajr.179.3.1790769.
[18] Gaerte SC, Meyer CA, Winer-Muram HT, Tarver RD, Conces DJ. Fat-containing lesions of the chest. Radiographics 2002;22 Spec No:S61–78. doi:10.1148/radiographics.22.suppl_1.g02oc08s61.